# Atmospheric $CO_2$ response to volcanic eruptions: The role of ENSO, season, and variability

Thomas Lukas Frölicher,[1,2] Fortunat Joos,[1,3] Christoph Cornelius Raible,[1,3] and Jorge Louis Sarmiento[2]

[1] Tropical explosive volcanism is one of the most important natural factors that significantly impact the climate system and the carbon cycle on annual to multi-decadal time scales. The three largest explosive eruptions in the last 50 years—Agung, El Chichón, and Pinatubo—occurred in spring/summer in conjunction with El Niño events and left distinct negative signals in the observational temperature and $CO_2$ records. However, confounding factors such as seasonal variability and El Niño-Southern Oscillation (ENSO) may obscure the forcing-response relationship. We determine for the first time the extent to which initial conditions, i.e., season and phase of the ENSO, and internal variability influence the coupled climate and carbon cycle response to volcanic forcing and how this affects estimates of the terrestrial and oceanic carbon sinks. Ensemble simulations with the Earth System Model (Climate System Model 1.4-carbon) predict that the atmospheric CO2 response is ~60% larger when a volcanic eruption occurs during El Niño and in winter than during La Niña conditions. Our simulations suggest that the Pinatubo eruption contributed $11 \pm 6\%$ to the 25 Pg terrestrial carbon sink inferred over the decade 1990–1999 and $-2 \pm 1\%$ to the 22 Pg oceanic carbon sink. In contrast to recent claims, trends in the airborne fraction of anthropogenic carbon cannot be detected when accounting for the decadal-scale influence of explosive volcanism and related uncertainties. Our results highlight the importance of considering the role of natural variability in the carbon cycle for interpretation of observations and for data-model intercomparison.

**Citation:** Frölicher, T. L., F. Joos, C. C. Raible, and J. L. Sarmiento (2013), Atmospheric $CO_2$ response to volcanic eruptions: The role of ENSO, season, and variability, *Global Biogeochem. Cycles, 27*, 239–251, doi:10.1002/gbc.20028.

## 1. Introduction

[2] The atmospheric $CO_2$ record measured at Mauna Loa [*Keeling et al.*, 2001] shows considerable variability on interannual to decadal time scales associated with major volcanic eruptions [*Jones and Cox*, 2001; *Frölicher et al.*, 2011; *Brovkin et al.*, 2010] and ENSO events [*Bacastow et al.*, 1980; *Feely et al.*, 1999]. The origin of this variability and underlying mechanisms, however, are less well understood and quantified than the centennial increase due to human-induced carbon emissions from fossil fuel and land-use change. A reason is the lack of or the brevity of spatially and temporarily resolved observational records. In addition,

Earth System Modelers have only recently started to employ ensemble simulations for the coupled carbon-climate system to investigate the role of internal variability [e.g. *Frölicher et al.*, 2009] and related analyses are largely missing in the peer reviewed literature, thereby lagging behind the physical climate modeling community. A quantitative understanding of natural internal and externally forced variability is, however, a prerequisite to detect decadal-to-centennial-scale climate and carbon cycle trends, to properly attribute such trends to anthropogenic and natural forcings from the often short instrumental records, and to facilitate a meaningful evaluation of Earth System Models with observations.

[3] Internal variability is the natural variability of the climate system that occurs in the absence of external forcing. The internal variability, or so-called chaotic component of the climate system, includes processes intrinsic to the atmosphere, the ocean, and the coupled atmosphere-ocean system [*Deser et al.*, 2012]. An ensemble approach provides a powerful tool for quantifying internal variability. Ensemble simulations are multiple realizations that are forced by identical boundary conditions (e.g., volcanic eruptions) but started from different initial conditions. The central idea is that with a sufficient number of ensemble simulations, with the modes of variability randomized, the ensemble mean can be used to evaluate the deterministic response of the climate system to volcanic

[1]Climate and Environmental Physics, Physics Institute, University of Bern, Bern, Switzerland.
[2]Program in Atmospheric and Oceanic Sciences, Princeton University, Princeton, New Jersey, USA.
[3]Oeschger Centre for Climates Change Research, University of Bern, Bern, Switzerland.

Corresponding author: T. L. Frölicher, Program in Atmospheric and Oceanic Sciences, Princeton University, 300 Forrestal Road, Sayre Hall, Princeton, NJ 08544, USA. (tfrolich@princeton.edu)

eruptions. In a complementary way, the spread of the ensemble distribution can provide an estimate of the envelope of internal variability that is superimposed on the deterministic response to volcanic eruptions.

[4] Approximately 40% of the uncertainty related to warming projected over the 21st century stems from the uncertainties associated with the carbon cycle [*Meehl et al.*, 2007]. A key question is how much the land and ocean will continue to absorb anthropogenic $CO_2$. A diagnosed positive trend in the airborne fraction, the ratio of $CO_2$ accumulating in the atmosphere to the total anthropogenic $CO_2$ emissions (fossil fuel and cement, plus land emissions), has been used by authors of the Global Carbon Project to argue that the sink efficiency of the land and ocean carbon sinks at absorbing excess $CO_2$ has decreased [*Canadell et al.*, 2007; *Le Quéré et al.*, 2009]. Recent studies, however, challenge the existence of an increasing trend in the airborne fraction [*Knorr*, 2009], and others question whether it can be interpreted as indicating a decrease in the efficiency of the carbon sinks [*Gloor et al.*, 2010; *Sarmiento et al.*, 2010; *Rafelski et al.*, 2009]. *Gloor et al.* [2010] and *Knorr* [2009] show that the noise in the observation data and the uncertainties in land use emission estimates are too large to detect trends in the airborne fraction. In addition, several factors such as non-exponential growths of carbon emissions, changes in the response of the carbon sinks to rising $CO_2$ and climate, and natural variability (e.g., El Niño-Southern Oscillation or volcanic eruptions) influence the variability of the diagnosed airborne fraction [*Gloor et al.*, 2010; *Sarmiento et al.*, 2010; *Rafelski et al.*, 2009]. Thus, the airborne fraction is a relatively poor diagnostic for analyzing changes in the carbon sink efficiency. A quantitative attribution analysis of airborne fraction trends to different mechanisms, however, is missing in the peer-reviewed literature.

[5] The goal of this study is to quantify the role of volcanic forcing in shaping interannual-to-decadal variability in atmospheric $CO_2$ and carbon sinks and to highlight interdependencies with the ENSO, the seasonal cycle, and the role of internal variability. By properly accounting for the influence of volcanic eruptions on atmospheric $CO_2$ trends, we contribute to the ongoing debate over whether a slowdown of the land and ocean in sequestering anthropogenic carbon is already detectable.

[6] Volcanoes contribute to the interannual to multi-decadal variability of the carbon cycle and the climate system [*Robock*, 2000]. In the period of available direct atmospheric $CO_2$ measurement data, after 1958, there were three large tropical volcanic eruptions (Agung in March 1963 at 8°S, El Chichón in April 1982 at 17°N, and Pinatubo in June 1991 at 15°N). All three eruptions occurred in conjunction with a strong El Niño event in boreal spring/summer, and observations show a drop in global mean surface air-temperature and atmospheric $CO_2$. In general, the land biosphere increases carbon uptake during cool climate volcanic events [*Jones and Cox*, 2001; *Frölicher et al.*, 2011]. However, the extent to which initial conditions and internal variability are important for the carbon cycle response to volcanic eruptions is currently not known.

[7] In this study, we use a fully coupled Earth System Model to assess the impact of volcanic eruptions on the physical climate system and the carbon cycle. Sensitivity studies are carried out by imposing a volcanic eruption either in boreal summer or winter, or in association with El Niño or La Niña. We show that the carbon system response critically depends on these initial states, particularly in the first few years after the eruption. We investigate how $CO_2$ would have evolved over the past 50 years in the absence of eruptions and attribute trends in the airborne fraction to volcanic eruptions and related uncertainties. We show that natural variability related to explosive volcanic eruptions and internal climate modes must be considered for a reliable interpretation of observed trends and to arrive at robust conclusions regarding changes in carbon sinks.

[8] The rest of this paper is organized as follows: section 2 presents the model used in this study and the experimental design. The results are described in section 3. A comparison with observationally based carbon fluxes after the Pinatubo eruption and a discussion about the implications for the global carbon budget is presented in section 4. The conclusions are presented in section 5. Details of the calculation of the volcanic signal in the observed temperature and $CO_2$ records, and the calculation of the airborne fraction are presented in Appendix A and Appendix B.

## 2. Methods

### 2.1. Model

[9] Simulations were performed with the coupled climate-carbon cycle model of the National Centre for Atmospheric Research (NCAR) Climate System Model (CSM) 1.4-carbon [*Fung et al.*, 2005; *Doney et al.*, 2006; *Frölicher et al.*, 2009; *Frölicher and Joos*, 2010]. The core of the model consists of ocean, atmosphere, land, and sea ice physical components. CSM1.4-carbon includes a modified version of the Carnegie-Ames-Stanford Approach terrestrial biogeochemistry model, termed CASA′, and a derivative of the Ocean Carbon Intercomparison Project 2 oceanic biogeochemistry model. CASA′ incorporates three live vegetation pools and nine dead carbon pools. Autotrophic respiration is not explicitly modeled and is assumed to be 50% of gross primary production. Heterotrophic respiration and carbon flow in litter and soil organic matter pools vary with soil temperature and moisture. Turnover times range from 20 days for the metabolic soil pool to 500 years for the passive pool. The average turnover time scale of less than 5 years of 60% of the soil carbon pools in the NCAR CSM1.4-carbon model is consistent with flux-weighted times derived from radiocarbon measurements [*Fung et al.*, 2005; *Trumbore*, 2000].

[10] Details on strengths and weaknesses of the model can be found in the peer-reviewed literature [*Doney et al.*, 2006; *Schneider et al.*, 2008; *Frölicher et al.*, 2009; *Frölicher and Joos*, 2010; *Steinacher et al.*, 2010] where modeled physical and biogeochemical fields are discussed and compared with observations. The carbon cycle response of the model to very large volcanic eruptions is described in *Frölicher et al.* [2011]. They show that strong reduction in heterotrophic respiration leads to enhanced carbon uptake in tropical regions after volcanic eruptions. This finding is in line with previous studies [*Jones and Cox*, 2001; *Brovkin et al.*, 2010]. We extend the existing evaluation by analyzing simulated interannual variability in atmospheric $CO_2$ of the NCAR CSM1.4-carbon model (Figure 1). Overall, the model captures the observed interannual variability reasonably well.
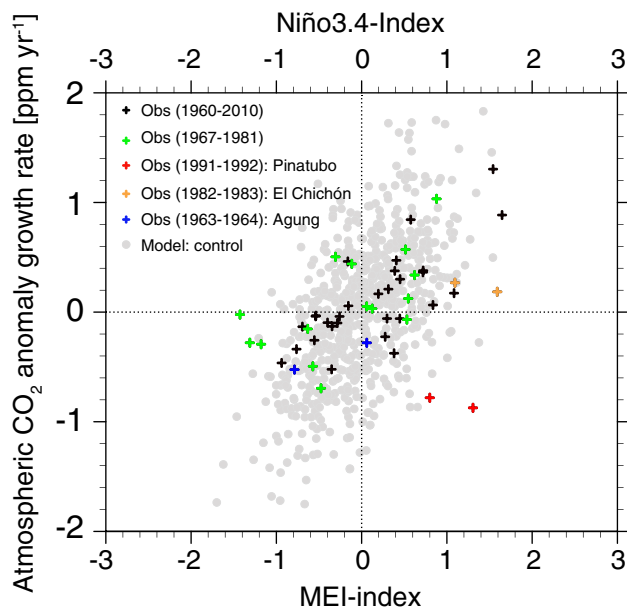
**Figure 1.** Scatterplot of modeled annual mean atmospheric $CO_2$ growth rates anomalies against sea surface temperature anomalies in the Niño3.4 index region from a 680 year control simulation of the NCAR CSM1.4-carbon model. Observed annual mean atmospheric $CO_2$ growth rates anomalies at Mauna Loa against the MEI index are also included. The annual mean atmospheric $CO_2$ growth rate has been corrected first for the anthropogenic influence.

The data over the volcano-free period 1967–1981 show a linear regression coefficient of 0.38 ppm $yr^{-1}$ per multivariate ENSO index (MEI) change ($r^2 = 0.38$; green crosses in Figure 1). The linear regression coefficient is slightly smaller when including all data from 1960 to 2010 (all crosses in Figure 1). The model shows a regression coefficient of 0.58 ppm $yr^{-1}$ per Niño3.4-index change ($r^2 = 0.48$; grey dots in Figure 1) obtained from a 680 year pre-industrial control simulation. Large carbon releases during El Niño conditions are simulated in tropical land regions, particularly in the northern part of South America, South East Asia, India, and tropical Africa. This is qualitatively in good agreement with observationally based estimates [e.g., *Rödenbeck et al.*, 2003]. The ocean carbon cycle response to ENSO is marginal in the NCAR CSM1.4-carbon model. In contrast to observationally based estimates [*Feely et al.*, 1999], largest variability in air-sea fluxes is simulated in the Southern Ocean and North Atlantic and seems not to be associated with ENSO. This is caused by overly strong iron limitation in the tropical Pacific Ocean in the model and therefore low surface biological uptake [*Doney et al.*, 2006; *Schneider et al.*, 2008; *Steinacher et al.*, 2010]. *Feely et al.* [1999] showed that the normally prevailing strong outgassing of $CO_2$ in the equatorial Pacific during an El Niño is reduced due to increased sea surface temperature and decreased supply of nutrient and carbon-rich water by upwelling.

## 2.2. Experimental Design

[11] Four sets of six-member ensemble perturbation simulations with identical volcanic forcing targeted to match the aerosol optical depth changes caused by the Pinatubo eruption were performed with the NCAR CSM1.4-carbon model (Table 1). Six ensemble members are sufficient to represent internal variability in global mean atmospheric $CO_2$. A larger number of ensembles do not yield a bigger uncertainty range. The ensemble spread, measured as one standard deviation in simulated atmospheric $CO_2$ averaged over the first 10 years in the El Niño summer cases, is 0.47 ppm and 0.48 ppm when using four and six ensemble members, respectively. The simulations are carried out by imposing a volcanic eruption either in boreal summer (1 July) or winter (1 January), or in association with El Niño or La Niña. Initial conditions are chosen based upon the phase of the model's own season and ENSO phase from selected points in a quasi-stable preindustrial control simulation. El Niño (La Niña) initial conditions are randomly chosen when the Niño3.4 index [*Trenberth*, 1997] exceeds ±0.4°C for at least 9 months in the control simulation. The initial conditions are separated by at least 11 years, which leads to substantially different climate states for each ensemble member. Each ensemble member is perturbed by the similar strength and pattern as the Mount Pinatubo eruption in 1991. The volcanic forcing, which is identical in all simulations, is introduced to the model as prescribed evolution of monthly zonal mean stratospheric aerosol optical depth following *Ammann et al.* [2003] (Figure 1a in *Frölicher et al.* [2011]). Thus, potential differences in the atmospheric spread of volcanic aerosols due to season or internal variations of the stratospheric circulation are neglected. The simulated response in climate results from changes in aerosol optical depth and related changes in energy fluxes. The $CO_2$ response is a consequence of the altered physical climate as direct $CO_2$ emissions by recent volcanic eruptions are negligible and accounted for less than 0.15% of today's $CO_2$ emissions [*Gerlach*, 2011]. Potential effects of tropospheric volcanic aerosols on cloud formation are not included.

[12] The baselines of the sensitivity simulations are delivered by a control simulation for perpetual 1820 pre-industrial conditions [*Doney et al.*, 2006]. From each ensemble member, the corresponding 10 year period from the control simulation is subtracted. This procedure guarantees that the "pure" volcanic-induced response of the climate and the carbon cycle is extracted. Then, the ensemble mean and one standard deviation of the ensemble are calculated. The degree of internal variability was measured as the spread (one standard deviation) between the individual members of the ensemble during the integration period.

**Table 1.** Overview of All Simulations Conducted for This Study[a]

| Experiment | Ensembles | Pinatubo forcing | Initial Conditions | Years |
|---|---|---|---|---|
| El Niño winter | 6 | 1X | El Niño and winter | 10 |
| | 6 | - | El Niño and winter | 10 |
| La Niña winter | 6 | 1X | La Niña and winter | 10 |
| | 6 | - | La Niña and winter | 10 |
| El Niño summer | 6 | 1X | El Niño and summer | 10 |
| (standard run) | 6 | - | El Niño and summer | 10 |
| La Niña summer | 6 | 1X | La Niña and summer | 10 |
| | 6 | - | La Niña and summer | 10 |

[a]The number of ensemble members, the Pinatubo scaling, the initial conditions, and the lengths of the simulations. All experiments start from nearly steady state pre-industrial conditions.

## 3. Results

[13] The simulations starting with El Niño and boreal summer initial conditions (standard runs) mimic the observed overlap of the Agung, El Chichón, and Pinatubo eruption with El Niño and summer conditions. We will focus our discussion first on these standard runs. The ensemble mean of the standard runs yields a decrease in global mean atmospheric surface air temperature and atmospheric $CO_2$ of $0.42 \pm 0.37°C$ and $1.64 \pm 0.26$ ppm, respectively (green lines in Figures 2a and 2b). The temperature decrease in the standard runs is consistent with the observation-based estimate [*Thompson et al.*, 2009], whereas the global mean $CO_2$ decrease at the peak underestimates the observation-based
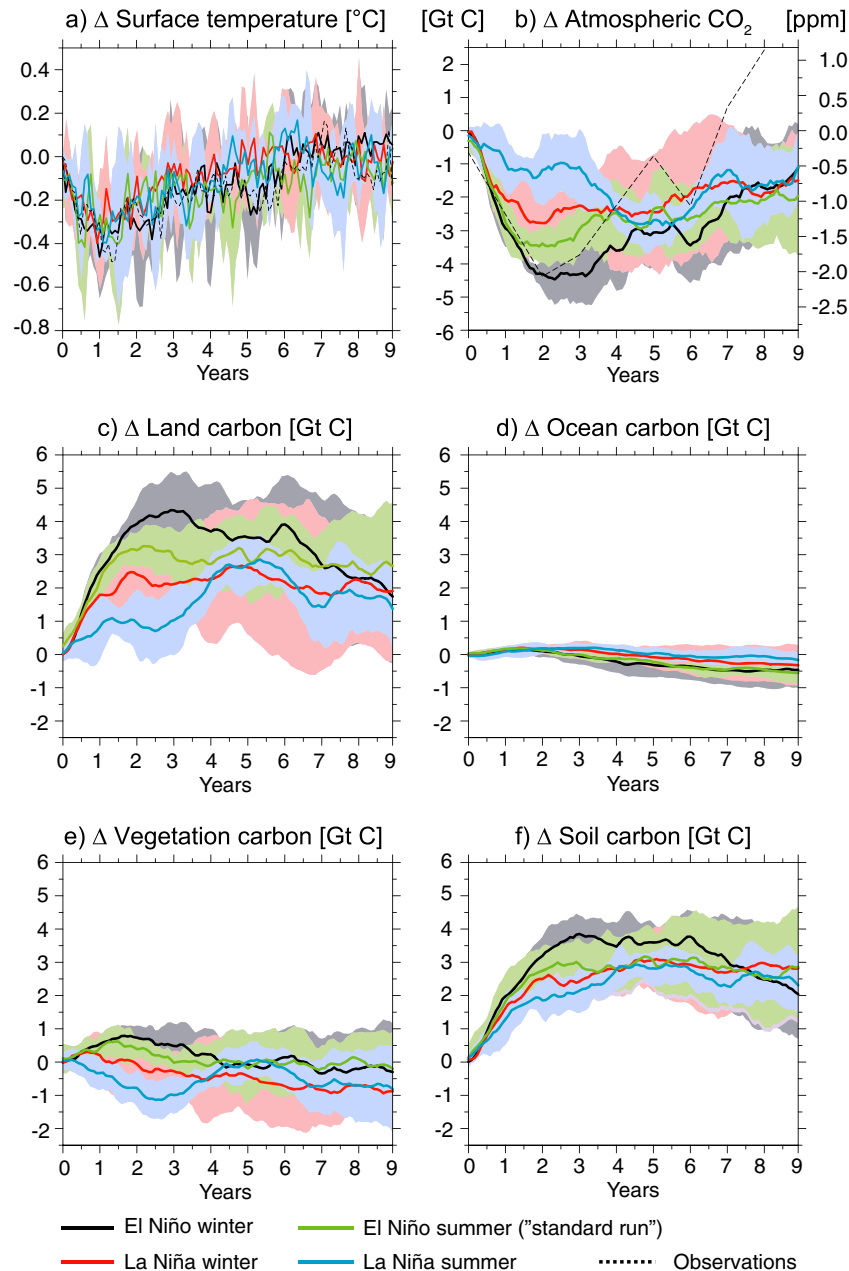


**Figure 2.** Simulated global mean changes after the Pinatubo eruption. Temporal evolution of global ensemble monthly mean differences in (a) atmospheric surface temperature, (b) atmospheric $CO_2$, (c) land carbon inventory, (d) ocean carbon inventory, (e) vegetation carbon inventory, and (f) soil carbon inventory between six simulations with and without volcanic eruptions is shown. The eruptions started in El Niño winter (black), La Niña winter (red), El Niño summer (green), and La Niña summer (blue) conditions. Shadings indicate one standard deviation confidence interval of the ensemble simulations. Dashed black lines indicate observation-derived temperature and atmospheric $CO_2$ changes after the Mount Pinatubo eruption. Note that the calculation of the observation-derived atmospheric $CO_2$ changes must be viewed as a tentative attempt (Appendix A).

estimate by about 19% (dashed black lines in Figures 2a and 2b). It is very difficult, however, to estimate amplitude, timing, and recovery of the atmospheric $CO_2$ anomaly from observations as it is based on several assumptions (see Appendix A for more details). Thus the observational-based estimate must be viewed as a tentative attempt. The underestimation may also be related to the neglect of changes in the fraction of diffusive radiation in the primary productivity algorithm of the NCAR CSM1.4-carbon model; an increase in the diffusive radiation as seen after volcanic eruptions may boost productivity in the first few years and thus carbon uptake by alleviating light limitation [*Gu et al.*, 2003; *Mercado et al.*, 2009]. Alternatively, the underestimation may point to a low carbon cycle-climate sensitivity on the multi-year time scale of the NCAR CSM1.4-carbon model, which has been identified in transient historical simulations for this model (4.3 ppm/°C) [*Frölicher et al.*, 2011]. This suggests that our simulated $CO_2$ response to volcanic forcing and internal variability estimates is rather at the lower bound. A larger number of ensembles may not yield a bigger uncertainty range, as the ensemble spread does not significantly decrease when using four instead of six ensemble members.

[14] Temperature anomalies in all cases last up to 7 years (Figure 2a)—much longer than the pure volcanic-induced total surface energy flux changes. The perturbations in $CO_2$ are multi-decadal (Figures 2b–2f). Nine years after the perturbation, the land carbon pools are perturbed by 2.6 Gt C in the El Niño summer case (Figure 2c). Thus, the land carbon pool changes account for about 130% of the total $-2.0$ Gt C atmospheric $CO_2$ perturbation after 9 years. Most of the carbon is taken up by the soil carbon pools while the vegetation carbon pools show small changes (Figures 2e and 2f). In comparison to the land, the ocean inventory changes are much smaller (Figure 2d). The ocean initially absorbs carbon mainly in response to cooling, but turns into a source after a couple of years in response to the lowered atmospheric $CO_2$ [*Brovkin et al.*, 2010; *Frölicher et al.*, 2011]. Thus, the ocean compensates somewhat the long-term decrease in atmospheric $CO_2$ due to land carbon inventory increases.

[15] Next, we analyze the aspects of the terrestrial model that leads to the long-tail response in the land carbon inventory in the standard case (Figure 3). In general, a small

increase in net primary production (NPP) in the tropics (Figure 3a) leads to an enhanced carbon flux from the vegetation carbon pools to the soil pools. The related increase in soil carbon inventory is amplified by the slower decay rate of soil carbon due to temperature and soil moisture changes (Figure 3b). Thus, tropical soil carbon pools with a slowly decomposing time scale of several years remain significantly perturbed by the end of the simulation (Figure 3b).

[16] Next, we compare all sensitivity simulations. In contrast to the surface energy flux, temperature (Figure 2a), and precipitation, the amplitude and timing of the atmospheric $CO_2$ response are strongly sensitive to the initial ENSO phase and season (Figure 2b). The $CO_2$ response is larger ($-2.11 \pm 0.39$ ppm) with a maximum after 2–3 years with El Niño and boreal winter initial conditions, whereas the response is smaller ($-1.31 \pm 0.48$ ppm) with a maximum after 4–5 years with La Niña and boreal summer starting conditions. The impact of initial conditions diminishes with time, as the four different cases converge to similar states after 4–5 years.

[17] Differences in atmospheric $CO_2$ between the cases can be attributed to differences in global mean terrestrial vegetation and soil carbon inventory changes (black and blue lines in Figure 2e and 2f). These changes are in turn driven by changes in NPP and heterotrophic respiration ($R_h$) in the first four years after the volcanic eruption (Figure 4). Globally, $R_h$ is suppressed in all cases, whereas the sign of NPP changes varies between the cases. The differences in the atmospheric $CO_2$ response between the cases are thus caused by different NPP responses in the NCAR CSM1.4-carbon model. For example, NPP increases during the first 2 years in the El Niño winter case which, together with a decrease in $R_h$, leads to a large atmospheric $CO_2$ response. In the La Niña summer case, however, both NPP and $R_h$ decrease and the simulated atmospheric $CO_2$ anomaly is small. Averaged over the first 4 years, El Niño cases tend to have enhanced NPP after a volcanic eruption (El Niño winter: 0.46 Gt C/yr; El Niño summer: 0.17 Gt C/yr; Figures 4a and 4b) and reduced $R_h$ (El Niño winter: $-0.44$ Gt C/yr; El Niño summer: $-0.46$ Gt C/yr; Figures 4a and 4b), whereas La Niña cases tend to have both reduced NPP (La Niña winter: $-0.23$ Gt C/yr; La Niña summer: $-0.43$ Gt C/yr; Figures 4c and 4d) and reduced $R_h$ (La Ninã winter: $-0.80$ Gt C/yr; La
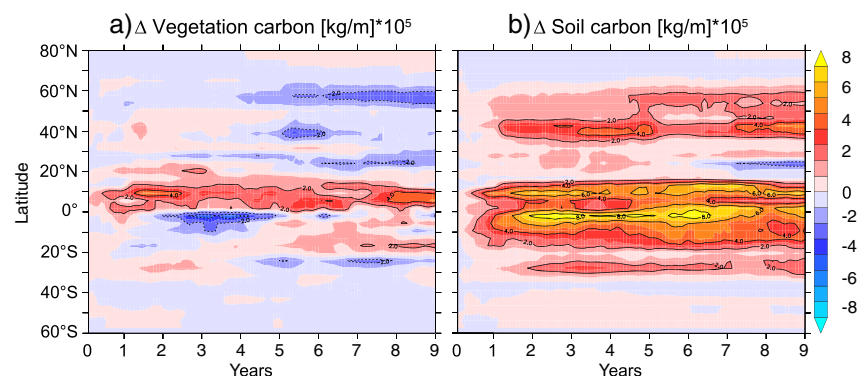


**Figure 3.** Simulated land carbon inventory changes after the Pinatubo eruption in the El Niño summer case. (a) Temporal evolution of zonally integrated ensemble monthly mean differences in vegetation carbon between six simulations with and without volcanic eruptions started in El Niño summer conditions. (b) Same as Figure 3a, but for soil carbon.
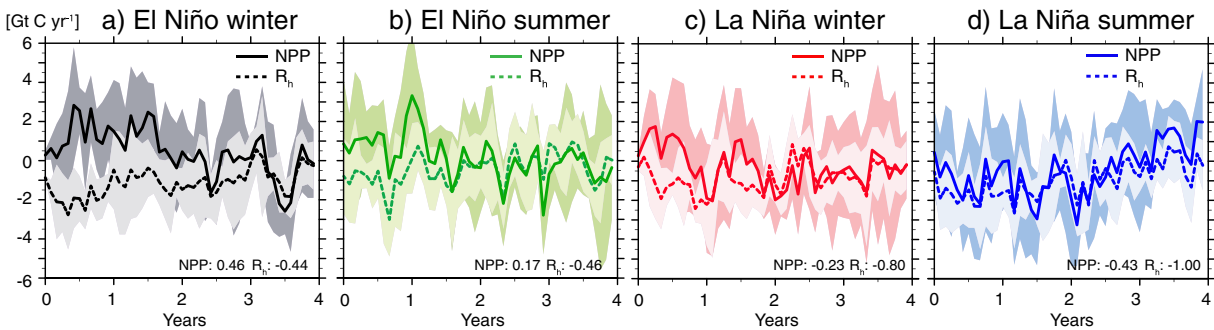
**Figure 4.** Temporal evolution of simulated global integrated ensemble monthly mean net primary production and heterotrophic respiration changes between six simulations with and without volcanic eruptions. Pinatubo eruption started in (a) El Niño winter, (b) El Niño summer, (c) La Niña winter, and (d) La Niña summer conditions. Shadings indicate one standard deviation confidence interval of the ensemble simulations. Numbers in all panels show NPP and $R_h$ changes in Gt C/yr averaged over the first 4 years after the volcanic eruption.

Niña summer: $-1.00$ Gt C/yr; Figures 4a and 4b). Winter cases also tend to have larger NPP than summer cases.

[18] On a regional scale, the differences in carbon uptake between the El Niño winter and La Niña summer case during the first 4 years after a volcanic eruption are located in the tropics and parts of North America and Europe (Figures 5a–5c).

[19] The NPP (Figures 5d–5f) changes are mainly a result of changes in precipitation (Figures 5j–5l) and soil moisture in the NCAR CSM1.4-carbon model. *Frölicher et al.* [2011] show a significant correlation between NPP and soil moisture in these regions after volcanic eruptions (see Figure 7 in *Frölicher et al.* [2011] for more details). Whereas drying (Figure 5l) and soil moisture decrease lead to a decrease in NPP (Figure 5f) in the La Niña summer case in parts of Africa and northeast South America, precipitation (Figure 5k) and soil moisture increase lead to a net increase in NPP (Figure 5e) in these regions in the El Niño winter cases. $R_h$ changes are driven by temperature and soil moisture changes in the NCAR CSM1.4-carbon model [Figure 7 in *Frölicher et al.*, 2011]. As volcanic-induced cooling occurs in all cases (Figures 5m–5o), $R_h$ decreases in all cases and in most regions (Figures 5g–5i). However, internal variability in NPP and $R_h$ is large on a regional scale and complicates a clean attribution of mechanism. Our results show that regional differences in climate response patterns associated with the state of ENSO and the seasonal cycle contribute globally to widespread land carbon cycle responses to volcanic eruptions.

## 4. Discussion

### 4.1. Comparison With Observationally Based Carbon Fluxes After the Pinatubo Eruption

[20] We compare simulated land and ocean carbon flux anomalies averaged over the first 2 years after the Pinatubo eruption with atmospheric inversion estimates based on atmospheric $CO_2$ measurements from *Bousquet et al.* [2000], *Rödenbeck et al.* [2003], and *Baker et al.* [2006] (Figure 6). Both data and models show that the land is mainly responsible for the large carbon uptake after Pinatubo. The inversion-based estimates indicate an anomalous global air-land carbon flux of 0.88–1.11 Gt C yr$^{-1}$ and an anomalous air-sea carbon flux of 0.09–0.25 Gt C yr$^{-1}$. This is comparable to the

simulated carbon flux in the El Niño summer case of $1.38 \pm 0.19$ Gt C yr$^{-1}$ for the land and $0.02 \pm 0.06$ Gt C yr$^{-1}$ for the ocean, when accounting for the large ensemble spread. The small mismatch may be related to the inclusion of the counterbalancing El Niño signal in the inversion-based estimates. On regional scales, however, partly conflicting results from the inversions make a quantitative evaluation of the model performance somewhat more difficult. Uncertainties in the inversion results arise from the underconstrained network of $CO_2$ observations, the choice of the atmospheric transport model, and the sampling network strategy in the inversion studies. Overall, our ensemble-mean results agree with the multi-model inversion estimates of *Baker et al.* [2006] with a large tropical land uptake and relatively small fluxes elsewhere. Individual ensemble members, however, are also consistent with the small tropical land fluxes inferred by *Rödenbeck et al.* [2003] and *Bousquet et al.* [2000]. The *Bousquet et al.* [2000] inversion shows a dipole structure with carbon uptake in North America and a large release in Eurasia, a feature that is not supported by the other two inversions and the model ensemble. Air-sea carbon flux anomalies are an order of magnitude smaller both in the inversion and in the ensemble simulations.

[21] The spread in regional fluxes from the ensemble simulations demonstrates that it is absolutely essential to consider the role of internal climate variability when comparing model with observation-based evidence to gauge model performance and to avoid premature conclusions. Here, each of the six El Niño summer simulations represents an equally likely evolution of the climate-carbon cycle system after the Pinatubo eruption. The ensemble of these six El Niño summer simulations as well as the ensemble of the combined 24 El Niño winter, El Niño summer, La Niña winter, and La Niña summer simulations suggests that a wide range of global and regional fluxes responses to a Pinatubo-like volcanic eruption is plausible.

### 4.2. Implications for the Global Carbon Budget

[22] The multi-decadal and nonlinear impact of volcanic eruptions on the global carbon cycle has important implications for the detection and attribution that are required in the context of the global carbon budget. Our results from
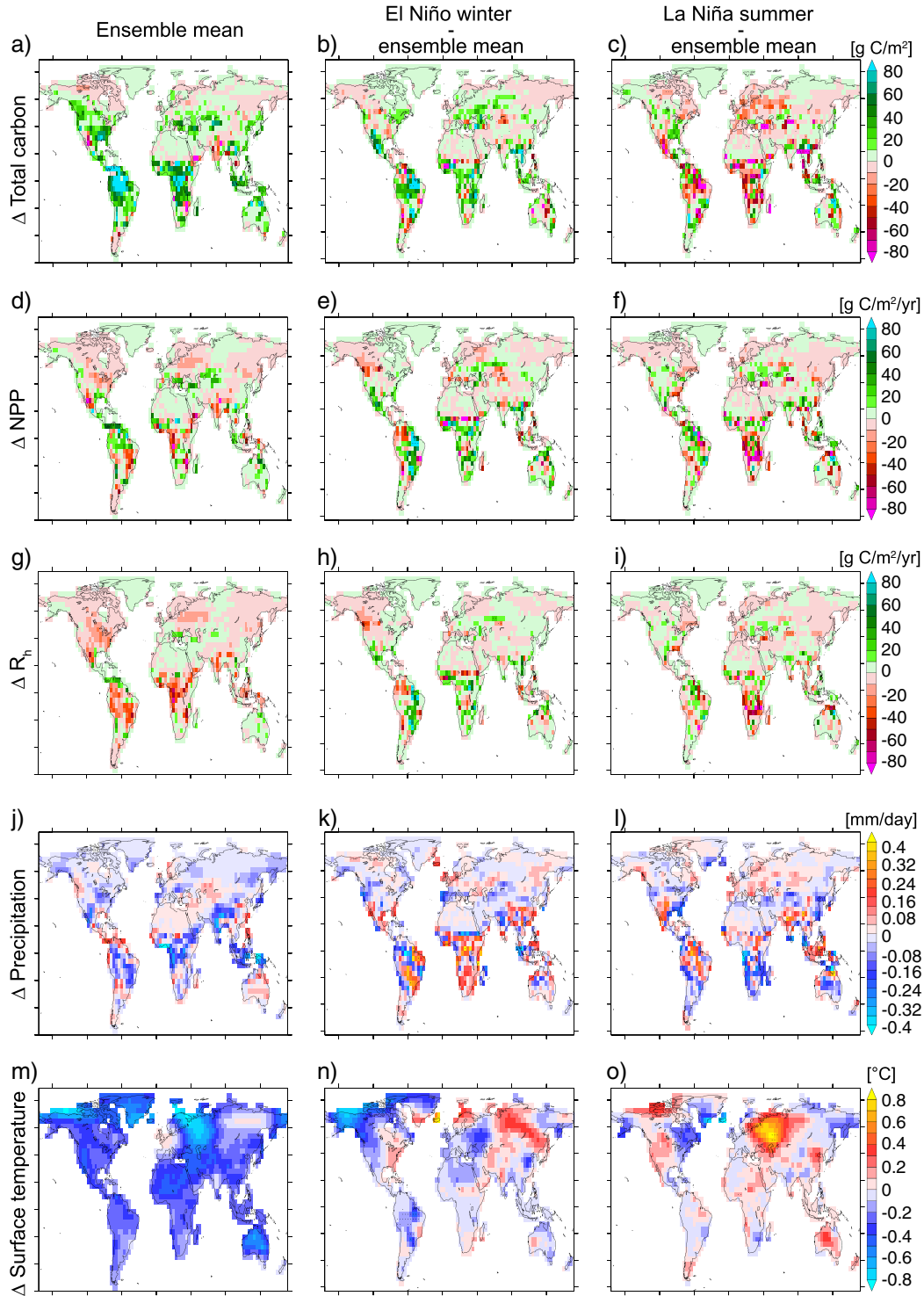
**Figure 5.** Simulated regional changes in (a–c) total carbon inventory, (d–f) net primary production, (g–i) soil respiration, (j–l) precipitation, and (m–o) surface temperature averaged over the first 4 years after the Pinatubo eruption. Shown are the differences between the ensemble mean of all 24 ensemble members and the corresponding control simulation (Figures 5a, 5d, 5g, 5j, and 5m), the ensemble mean of the anomalies of the six El Niño winter simulations and the ensemble mean of the anomalies of all 24 ensemble members (Figures 5b, 5e, 5h, 5k, and 5n), and the ensemble mean of the anomalies of the six La Niña summer cases and the ensemble mean of the anomalies of all 24 ensemble members (Figures 5c, 5f, 5i, 5l, and 5o).

the El Niño summer case suggest that the Pinatubo eruption contributed $2.7 \pm 1.6$ Pg C ($11 \pm 6\%$) to the 25 Pg land sink [*Pan et al.*, 2011] and $-0.4 \pm 0.2$ Pg C ($-2 \pm 1\%$) to the 22 Pg ocean carbon sink [*Le Quéré et al.*, 2009] in the 1990s. The internal variability, however, is large for both the land and the ocean.
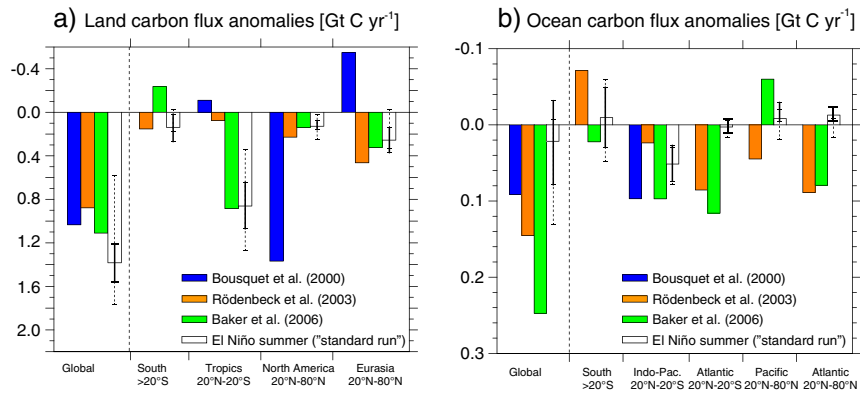
**Figure 6.** Simulated and observationally based carbon fluxes after the Pinatubo eruption are shown. (a) Air-land carbon fluxes for different regions after the Pinatubo eruption (positive: uptake of carbon through land biosphere; negative: release of carbon). (b) Same as Figure 6a, but for air-sea carbon fluxes. Shown are atmospheric inversion estimates (blue: *Bousquet et al.* [2000]; orange: run s90 with 19 sites from *Rödenbeck et al.* [2003]; and green: *Baker et al.* [2006]) and results from this study (white). Results for the NCAR CSM1.4-carbon model are calculated as the ensemble mean changes from the El Niño summer cases averaged over the first 24 months. Solid and dashed error bars indicate one standard deviation of the six El Niño summer cases and the 24 ensemble cases, respectively. Anomalies for the inversion results are calculated as differences between period June 1991 to May 1993 and June 1990 to May 1991. For each inversion, a 12 month running mean was first calculated to remove the seasonal cycle from the anomaly fluxes.

[23] To detect trends in the airborne fraction, the variability induced by volcanoes and ENSO needs to be removed from the atmospheric growth rate. Current studies [*Canadell et al.*, 2007; *Knorr*, 2009; *Le Quéré et al.*, 2009; *Gloor et al.*, 2010; *Sarmiento et al.*, 2010] assume that the volcanic signal in the atmospheric $CO_2$ record has time scales of a few years, related to short-term changes in aerosol optical depth changes, and that the atmospheric $CO_2$ concentration responds linearly to volcanic eruptions; thus no uncertainties are assigned to the responses. We quantify the uncertainty in the airborne fraction and its trend arising from decadal-scale nonlinear volcanic $CO_2$ signals by "correcting" the actual airborne fraction (month by month) for the influence of volcanic eruptions using our ensemble results in a probabilistic Monte Carlo approach (Figure 7). Two hundred sixteen volcano-free atmospheric $CO_2$ time series are generated by correcting the actual observed atmospheric $CO_2$ data at Mauna Loa with the $CO_2$ time series from our volcanic ensemble simulations (Figures 7a and 7b). The trends in the airborne fraction and the carbon sink fluxes are then calculated following the methodology outlined by *Raupach et al.* [2008]. A detailed description of the airborne fraction calculation and the Monte Carlo approach is given in Appendix B.

[24] We show that the trend in the "anthropogenic component of the airborne fraction" becomes negative when accounting for volcanoes by using our El Niño summer ensemble simulations (red line in Figure 7 and row 1 in column 6 of Table 2). The airborne fraction trend is slightly positive when no volcanic corrections are applied (row 5 in column 6 of Table 2). The magnitude of the airborne fraction trend depends on the scaling of the smaller Agung and El Chichón eruptions relative to Pinatubo and the correct magnitude of the $CO_2$ drop after a volcanic eruption. Smaller scaling factors for the Agung and El Chichón eruption resulted in smaller negative airborne fraction trends (row 2 in column

6 of Table 2 and green line in Figure 7). Larger $CO_2$ scaling for all volcanoes, by assuming that the NCAR CSM1.4-carbon model underestimates the true response, results in larger negative airborne fraction trends (row 3 in column 6 of Table 2 and blue line in Figure 7). The airborne fraction trends for all cases, however, are not significantly different from zero using a two sided $t$ test ($p$-value $< 0.05$).

[25] The uptake rates of the combined land and ocean carbon sink have increased over the last 50 years with an average trend of 1.40%/yr (Figure 7d and row 5 in column 7 of Table 2). When correcting for volcanoes, we show that trends in the uptake rates are even larger ($1.62 \pm 0.05$%/yr in our standard case; row 1 in column 7 of Table 2).

[26] It is well known that uncertainties in land use emission data are significant [e.g., *Houghton*, 2010]. Several papers pointed out that the ability to detect trends in the airborne fraction is heavily impacted by uncertainties in land use emission data [e.g., *Le Quéré et al.*, 2009]. To assess the implications of uncertainty in land use emission data for trends in airborne fraction and carbon sinks, we replaced the land use emission bookkeeping data from *Houghton* [2003] in our standard case with estimates from *Stocker et al.* [2011]. We bring the *Stocker et al.* [2011] land use emission estimates into discussions here, as these estimates include, in addition to the bookkeeping flux considered in the Houghton data, also land use feedback fluxes associated with changes in climate and atmospheric $CO_2$ [*Strassmann et al.*, 2008]. The Stocker et al. estimates are based on spatially explicit land use maps including cropland, pasture, and built areas, and were not included in earlier studies [e.g., *Le Quéré et al.*, 2009]. The trend in airborne fraction becomes only slightly less negative when using land use change estimates from *Stocker et al.* [2011] in comparison to the computed airborne fraction using the *Houghton* [2003] data (row 4 in Table 1 and yellow line in Figure 7). Thus, volcanic eruptions may have a larger impact
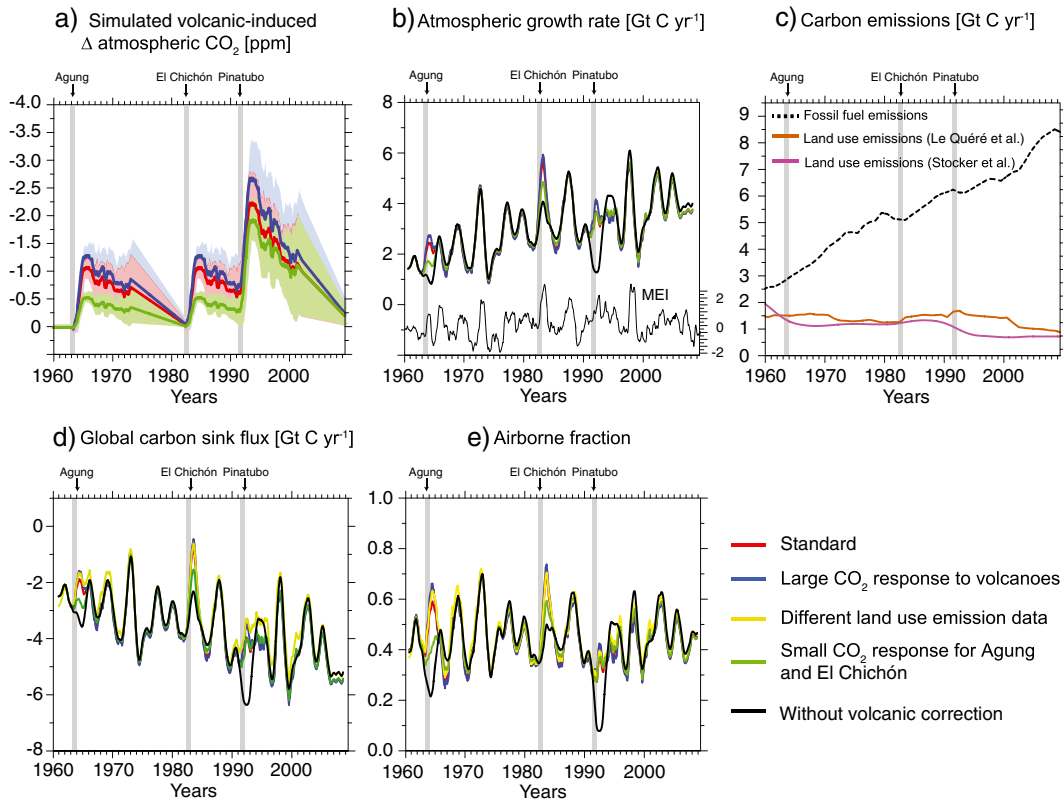
**Figure 7.** Components of the global carbon budget. Time series of (a) model-based atmospheric $CO_2$ anomalies resulting from volcanic eruptions, (b) atmospheric $CO_2$ growth rate as observed and after correcting for the influence of volcanic eruptions, (d) global carbon sink flux to the ocean and land, and (e) airborne fraction over the period 1960–2009 as summarized and described in Table 2. The monthly time series in Figures 7b, 7d, and 7e are filtered with a 15 month running mean. (c) Carbon emissions from fossil fuel combustion and cement production (black) and from land use change as given by *Le Quéré et al.* [2009] (brown) and *Stocker et al.* [2011] (purple). The shaded areas in Figure 7a show one standard deviation confidence interval of the ensemble simulations. Thick black lines in Figures 7b, 7d, and 7e indicate time series that are calculated from the Mauna Loa $CO_2$ record without correcting for the influence of volcanic eruptions. The multivariate ENSO index (MEI) is also shown in Figure 7b. The three major volcanic eruptions Agung, El Chichón, and Pinatubo are identified by the grey vertical band in all panels.

on airborne fraction trend estimates than uncertainties in land use emission data.

[27] Our results are not directly comparable with the results of *Le Quéré et al.* [2009] (row 6 in Table 2) as they use monthly global volcanic aerosol index data as a measure of volcanically induced aerosol optical depth changes and as a proxy for the impact of volcanic eruption on the global carbon cycle. In earlier studies [*Le Quéré et al.*, 2009; *Canadell et al.*, 2007], a linear assumption between aerosol index data and atmospheric $CO_2$ growth rate is usually applied. Here, we show that this assumption may not be adequate as we found a much longer impact of volcanic eruption on the carbon cycle than 1–2 years, typically seen when using volcanic aerosol indices, and a large sensitivity on the pre-existing initial state of the atmospheric $CO_2$ response to volcanic eruptions.

## 5. Conclusions

[28] In this study, sensitivity simulations are carried out by imposing a volcanic eruption either in the boreal summer or

northern winter, or in association with El Niño or La Niña events to study the impact on the physical climate system and the carbon cycle. Implications for the global carbon budget are analyzed.

[29] Our analysis shows that the atmospheric $CO_2$ response to volcanic eruptions depends sensitively on the pre-existing climate state of the Earth system at the point of the eruption and the evolution of internal climate variability in the first years after the eruption. Furthermore, volcanic eruption produces perturbations to land carbon fluxes that extend for a decade or more.

[30] To our knowledge, volcanic sensitivity simulations with a fully coupled Earth System Model have not been used before to assess how atmospheric $CO_2$ would have evolved over recent decades in the absence of volcanic eruptions. This separation provides a first step toward an attribution analysis of causes of variations in ocean and land carbon sinks and the airborne fraction. Our analysis suggests that the decadal-scale volcanic effects are underestimated in recent studies describing airborne fraction trends [*Le Quéré et al.*, 2009; *Canadell et al.*, 2007]. Furthermore, we show

**Table 2.** Observation-Based Estimates of the Airborne Fraction of Anthropogenic $CO_2$ Emissions, Its Long-Term Trend, and Sensitivity of Results to Assumptions Regarding the Influence of Explosive Volcanic Eruptions and $CO_2$ Emissions From Land Use[a]

| | Airborne Fraction | | | | | Trend in Airborne Fraction | Trend in Global Carbon Sink Flux |
|---|---|---|---|---|---|---|---|
| | 1960–1969 | 1970–1980 | 1980–1990 | 1990–1999 | 2000 to Jun 2009 | Jan 1960 to Jun 2009 | Jan 1960 to Jun 2009 |
| *With volcano correction* | | | | | | | |
| Standard[b] | $0.46 \pm 0.01$[f] | $0.45 \pm 0.01$ | $0.46 \pm 0.02$ | $0.37 \pm 0.02$ | $0.45 \pm 0.02$ | $-0.17 \pm 0.07\%$/yr | $1.62 \pm 0.05\%$/yr |
| Small $CO_2$ response for Agung and El Chichón[c] | $0.44 \pm 0.01$ | $0.46 \pm 0.01$ | $0.46 \pm 0.01$ | $0.38 \pm 0.01$ | $0.46 \pm 0.02$ | $-0.05 \pm 0.05\%$/yr | $1.55 \pm 0.04\%$/yr |
| Large $CO_2$ response to volcanoes[d] | $0.47 \pm 0.02$ | $0.45 \pm 0.02$ | $0.46 \pm 0.03$ | $0.38 \pm 0.03$ | $0.45 \pm 0.02$ | $-0.23 \pm 0.09\%$/yr | $1.66 \pm 0.06\%$/yr |
| Different land use emission data[e] | $0.48 \pm 0.01$ | $0.47 \pm 0.01$ | $0.47 \pm 0.02$ | $0.41 \pm 0.02$ | $0.47 \pm 0.02$ | $-0.12 \pm 0.07\%$/yr | $1.53 \pm 0.05\%$/yr |
| *Without volcanic correction* | 0.41 | 0.47 | 0.45 | 0.37 | 0.48 | $0.15\%$/yr | $1.40\%$/yr |
| *Le Quéré et al.* [2009] | $0.39 \pm 0.07$ | $0.45 \pm 0.06$ | $0.48 \pm 0.05$ | $0.40 \pm 0.04$ | $0.45 \pm 0.04$[g] | $0.3 \pm 0.2\%$/yr[g] | |

[a]Airborne fractions from Table S1 in *Le Quéré et al.* [2009] over the period 1960–2008 are given for comparison. Trends in global carbon sink fluxes to the ocean and land are also given.
[b]El Niño summer cases; LUC estimates from *Houghton* [2003]; Agung and El Chichón $CO_2$ impact assumed to be 0.66 of Pinatubo.
[c]As standard, but Agung and El Chichón $CO_2$ impact assumed to be 0.33 of Pinatubo.
[d]As standard, but volcanic $CO_2$ impact for Agung, El Chichón and Pinatubo assumed to be 1.2 of standard.
[e]As standard but LUC estimates from *Stocker et al.* [2011].
[f]Values indicate $\pm$ one standard deviation.
[g]From 2000 to 2008.

that the omission of volcanoes is sufficient to explain the observed trend in the airborne fraction [*Gloor et al.*, 2010]. However, analysis of trends in the airborne fraction, as described in this study and elsewhere [*Le Quéré et al.*, 2009; *Canadell et al.*, 2007], is insufficient to make firm conclusions about whether the land and ocean uptake of anthropogenic carbon has slowed down due to recent climate change. As pointed out by *Gloor et al.* [2010], trends in the airborne fraction are not identical with changes in the ocean and land carbon sinks.

[31] Further volcano modeling studies will be needed to constrain our results in the quantitative details. Ensemble simulations are routinely used in the climate modeling community to quantify the amplitudes of the target signal (e.g., change in atmospheric $CO_2$ after volcanic eruptions) in comparison with the noise (internal variability), but ensemble simulations are not yet standard in the carbon cycle community. Our study may motivate analyses of observations for the coupled atmosphere-ocean-land system and model-observation comparison studies that take full account of the role of natural variability. The quantification of such variability is an essential step in distinguishing natural from human-induced perturbation of the carbon cycle-climate system. Future explosive volcanic eruptions have the potential to shed more light on Earth system response relationships and to narrow uncertainties in our quantitative understanding. Volcanic eruptions are of sufficient importance for process understanding so that observing systems on land and ocean should be able to resolve the fingerprints of the Earth system response to volcanic eruptions.

## Appendix A

[32] In this appendix, we provide details about the calculation of the volcanic signal in observed temperature and $CO_2$ records.

## Temperature

[33] We used three different time series from *Thompson et al.* 2009] (available at [http://www.atmos.colostate.edu/~davet/ThompsonWallaceJonesKennedy/): (i) the global mean monthly mean surface temperature $T_{obs}$, (ii) the ENSO-induced variability in global mean monthly mean surface temperature $T_{obs,ENSO}$, and (iii) the dynamically induced variability (e.g., through North Atlantic Oscillation) in global mean monthly mean surface temperature $T_{obs,dyn}$ (see Figure 4 in *Thompson et al.* [2009] for details). We calculated the pure volcanic signal in the temperature record as follows:

$$T_{obs,volc} = T_{obs} - T_{obs,ENSO} - T_{obs,dyn.}$$

Then, the anthropogenic trend (30 year linear trend centered on the June 1991 Pinatubo eruption) is subtracted from the residual time series.

## $CO_2$

[34] We used following three data sets to calculate the pure volcanic $CO_2$ signal in the $CO_2$ record: (i) the yearly atmospheric $CO_2$ data [*Keeling et al.*, 2001, given in column 2 of ftp://ftp.cmdl.noaa.gov/ccg/trends/co2_annmean_mlo.txt ], (ii) the yearly mean fossil fuel and cement emissions ($F_{foss}$) as well as the yearly mean land use emissions ($F_{luc}$) from *Le Quéré et al.* [2009] (available at http://lgmacweb.env.uea.ac.uk/lequere/co2/carbon_budget.htm), and (iii) the bimonthly MEI values from *Wolter and Timlin* [1993,1998] (available at http://www.esrl.noaa.gov/psd/people/klaus.wolter/MEI/table.html). Yearly series of total emission ($F_E = F_{foss} + F_{LUC}$) and MEI values are constructed.

[35] We calculated the pure volcanic $CO_2$ signal in the observations as follows:
[36] 1. The atmospheric growth rate in ppm month$^{-1}$ is calculated year (t) by year using the equation:

10

$$\mathrm{agr}(t) = CO_2(t) - CO_2(t-1).$$

[37] 2. We subtracted the contribution of emissions ($F_E$ in Pg C yr$^{-1}$; Figure 7c) from the atmospheric growth rate by using the assumption that 43% (average over period 1959–2006) of the emissions remain airborne:

$$\mathrm{agr_{emis\_cor}}(t) = \mathrm{agr}(t) - (0.43{*}F_E)\,/\,\gamma,$$

with $\gamma = 2.127$ Pg C/ppm.

[38] 3. We determined an approximate relationship over the "volcano-free" period 1967–1981 between the multivariate ENSO index (MEI; Figure 7b) and agr$_{emis\_cor}$ by using a linear regression (Figure 1):

$$\mathrm{agr_{emis\_cor}}(t) \cong 0.38 \times \mathrm{MEI}(t)\left(R^2 = 0.38\right).$$

[39] 4. By subtracting the MEI variations from agr$_{emis\_cor}$, we get an estimate of atmospheric $CO_2$ without ENSO-induced variability (agr$_{volc}$):

$$\mathrm{agr_{volc}}(t) = \mathrm{agr_{emis\_cor}}(t) - 0.38 \times \mathrm{MEI}(t).$$

[40] 5. $CO_2$ changes are then calculated as time-integrated changes of agr$_{volc}(t)$ relative to year 1990.

[41] We tried to get an uncertainty estimate of agr$_{volc}$ by (i) changing the constant airborne fraction from 43% to 40% and 46%, (ii) using a different land use estimate from *Stocker et al.* [2011], and (iii) using the entire time period 1960–2010 for the calculation of the linear regression coefficient between MEI and atmospheric $CO_2$ growth rate. The volcanic signal is marginally sensitive to the used airborne fraction (not shown), but using the *Stocker et al.* [2011] land use emissions and using the entire time period for linear regression leads to a slightly smaller magnitude of $CO_2$ peak and shorter recovery time. However, even after the correction for ENSO and emission, the time series agr$_{emis\_cor}$ shows large variability associated with volcanoes as well as internal variability making a clear isolation of the volcanic signal difficult to estimate. For example, the atmospheric growth rate in the late 1980s is anomalous low (approximately $-0.7$ ppm yr$^{-1}$) and has been associated with an abrupt increase in net land carbon uptake after 1988 [*Beaulieu et al.*, 2012]. Thus, this leads to small anomalies over the period 1991–2000 relative to 1990 and to a "fast recovery" in the observed atmospheric $CO_2$ signal. Finally, we assumed a linear relationship between MEI and atmospheric $CO_2$ growth rate as was done in previous analysis [*Raupach et al.*, 2008]. However, the strong El Niño years 1997 and 1998 (Figure 1; years 6 and 7 in Figure 2b) may lead to anomalous high $CO_2$ fluxes from tropical regions through enhanced biomass burning from recently exposed peat that is very sensitive to drought. The shoot-off in the high direction in the years 1997 and 1998 may therefore be caused by our linear relationship assumption that does not take into account nonlinearity.

## Appendix B

[42] In this appendix, we provide detail about the calculation of the airborne fraction. We calculated the trend in the airborne fraction as follows:

[43] 1. We generated 216 volcano-only monthly $CO_2$ time series over the period January 1960 to June 2010 ($CO_{2,\mathrm{volc}}$; Figure 7a). As we have six ensemble members (results from Figure 2b) and three eruptions (Agung, El Chichón, Pinatubo) during this time period, we got $n = 216$ ($6 \times 6 \times 6$) different evolutions of atmospheric $CO_2$ for the El Niño summer "standard run." We assumed that a volcanic signal lasts 20 years and extrapolated the time series from our experiments linearly to zero from year 10 to year 20 after the volcanic eruption. We scaled the simulated atmospheric $CO_2$ anomalies by 0.66 (and by 0.33 for sensitivity tests) for Agung and El Chichón as the observed aerosol optical depth changes for these volcanoes are two thirds of the Pinatubo.

[44] 2. We subtracted the n different simulated volcano-only monthly $CO_2$ times series over the period January 1960 to June 2010 from the observed smoothed deseasonalized atmospheric $CO_2$ record of *Keeling et al.* [2001] (data in column 8 of http://scrippsco2.ucsd.edu/data/in_situ_co2/monthly_mlo.csv) to get $n$ different "volcano-corrected" $CO_2$ time series:

$$CO_{2,\mathrm{volc\_cor}}{}^{(n)}(t) = CO_2(t) - CO_{2,\mathrm{volc}}{}^{(n)}(t).$$

[45] 3. We calculated the "volcano-corrected" atmospheric growth rates in Pg C yr$^{-1}$ (agr$_{volc\_cor}$; Figure 7b) for each time series $n$ as

$$\mathrm{agr_{volc\_cor}}{}^{(n)}(t) = (CO_{2,\mathrm{volc\_cor}}{}^{(n)}(t) - CO_{2,\mathrm{volc\_cor}}{}^{(n)}(t-1)){*}\gamma \, {*}1/\Delta t,$$

with $\gamma = 12{*}2.127$ PgC ppm$^{-1}$ and $\Delta t = 1/12$ years

[46] 4. To filter out the component of the atmospheric growth rate associated with ENSO, we first calculated the total surface atmospheric $CO_2$ sink flux ($F_{\mathrm{sinks,volc\_cor}}$; Figure 7d) for each time series $n$:

$$F_{\mathrm{sinks,volc\_cor}}{}^{(n)}(t) = \mathrm{agr_{volc\_cor}}{}^{(n)}(t) - F_E(t),$$

as the mechanistic links between ENSO and the $CO_2$ budget occur through the total (land plus ocean) surface-air exchange flux rather than through the atmospheric growth rate itself [*Raupach et al.*, 2008]. $F_E(t)$ are fossil fuel and land use emissions in Pg C yr$^{-1}$ (Figure 7c) and are obtained from Le Quéré (available at http://lgmacweb.env.uea.ac.uk/lequere/co2/carbon_budget.htm). A monthly series of total emission is constructed by linear interpolation of the annual emissions series thereby neglecting a small seasonal cycle in emissions. Uncertainties in the emissions estimates are not taken into account. The MEI-correlated component is then removed from $F_{\mathrm{sinks,volc\_cor}}$ for each time series $n$:

$$F_{\text{sinks,volc\_cor,mei\_cor}}^{(n)}(t) = F_{\text{sinks,volc\_cor}}^{(n)} - \mu^{(n)} \text{MEI}(t)$$

$\mu^{(n)}$ is the sensitivity of MEI to the $F_{\text{sinks,volc\_cor}}$ for each realization $n$. The bimonthly MEI values are obtained from *Wolter and Timlin* [1993,1998] (available at http://www. esrl.noaa.gov/psd/people/klaus.wolter/MEI/table.html) and are related to monthly values as described on the NOAA webpage.

[47] 5. The volcano- and MEI-corrected $CO_2$ airborne fractions ($\text{af}_{\text{volc\_cor,mei\_cor}}$) are then calculated for each time series $n$ as

$$\text{af}_{\text{volc\_cor,mei\_cor}}^{(n)}(t) = 1 + F_{\text{sinks,volc\_cor,mei\_cor}}^{(n)}(t)/F_E(t).$$

[48] 6. The linear trend of the airborne fraction ($r(\text{af}_{\text{volc\_cor,mei\_cor}})$) in units % $\text{yr}^{-1}$ is then calculated for each $\text{af}_{\text{volc\_cor,mei\_cor}}$ as

$$r\left(\text{af}_{\text{volc\_cor,mei\_cor}}\right)^{(n)} = \left(\text{af}_{\text{volc\_cor,mei\_cor}}\right)'(n)/\text{avg}\left(\text{af}_{\text{volc\_cor,mei\_cor}}^{(n)}\right)$$

with $(\text{af}_{\text{volc\_cor,mei\_cor}})'$ as the slope and $\text{avg}(\text{af}_{\text{volc\_cor,mei\_cor}})$ as the mean over the time period. The linear trend of the carbon sink fluxes has been calculated accordingly.

[49] 7. The statistical significance of the linear trend of each time series $n$, $(\text{af}_{\text{volc\_cor,mei\_cor}})'^{(n)}$, is calculated using two-sided Student's $t$ test ($p$-value $< 0.05$). Autocorrelation in the time series has been neglected, as significance levels are low for all cases.

[50] Additionally, we used the land use emissions estimate from *Stocker et al.* [2011] (not used in *Le Quéré et al.* [2009]) to calculate the airborne fraction. The land use emission estimates are first filtered with a spline using a cutoff period of 15 years. Note that we assume constant land emissions for the period 2004-2009 (Figure 7c).

## References

Ammann, C. M., G. A. Meehl, W. M. Washington, and C. S. Zehnder (2003), A monthly and latitudinally varying volcanic forcing dataset in simulations of 20th century climate. *Geophys. Res. Lett.*, *30*, doi:10.1029/2003GL016875.

Bacastow, R. B., J. A. Adams, C. D. Keeling, D. J. Moss, T. P. Whorf, and C. S. Wong (1980), Atmospheric carbon dioxide, the Southern Oscillation, and the weak 1975 El Niño. *Science*, *210*, 66–68, doi:10.1126/science.210.4465.66.

Baker, D. F., et al. (2006), TransCom 3 inversion intercomparison: Impact of transport model errors on the interannual variability of regional $CO_2$ fluxes, 1988–2003. *Global Biogeochem. Cycles*, *20*, GB1002, doi:10.1029/2004GB002439.

Beaulieu, C., J. L. Sarmiento, S. Mikaloff Fletcher, J. Chen, and D. Medvigy (2012) Identification and characterization of abrupt changes in the land

uptake of carbon. *Global Biogeochem. Cycles*, *26*, GB1007, doi:10.1029/2010GB004024.

Bousquet, P., P. Peylin, P. Ciais, C. Le Quéré, P. Friedlingstein, and P. P. Tans (2000), Regional changes in carbon dioxide fluxes of land and oceans since 1980. *Science*, *290*, 1342–1346, doi:10.1126/science.290.5495.1342.

Brovkin, V., S. J. Lorenz, J. Jungclaus, T. Raddatz, C. Timmreck, C. H. Reick, J. Segschneider, and K. Six (2010), Sensitivity of a coupled climate-carbon cycle model to large volcanic eruption during the last millennium. *Tellus B*, *62*, 674–681, doi:10.1111/j.1600-0889.2010.00471.x.

Canadell, J. P., C. Le Quéré, M. R. Raupach, C. B. Field, E. T. Buitenhuis, P. Ciais, T. J. Conway,N. P. Gillett, R. A. Houghton, and G. Marland (2007), Contributions to accelerating atmospheric $CO_2$ growth from economic activity, carbon intensity, and efficiency of natural sinks. *Proc. Natl. Acad. Sci. USA*, *104*(47), 18866–18870, doi:10.1073/pnas.0702737104.

Deser, C., A. S. Phillips, V. Bourdette, and H. Teng (2012), Uncertainty in climate change projections: The role of internal variability. *Clim. Dynam.*, *38*, 527–546, doi:10.1007/s00382-010-0977-x.

Doney, S. C., K. Lindsay, I. Fung, and J. John (2006), Natural variability in a stable 1000-yr global coupled climate-carbon cycle simulation. *J. Climate*, *19*, 3033–3054, doi:10.1175/JCLI3783.1, doi:10.1175/JCLI3783.1.

Feely, R. A., R. Wanninkhof, T. Takahashi, and P. Tans (1999), Influence of El Niño on the equatorial Pacific contribution to atmospheric $CO_2$ accumulation. *Nature*, *398*, 597–601, doi:10.1038/19273.

Frölicher, T. L., F. Joos, G.-K. Plattner, M. Steinacher, and S. C. Doney (2009), Natural variability and anthropogenic trends in oceanic oxygen in a coupled carbon cycle-climate model ensemble. *Global Biogeochem. Cycles*, *23*, GB1003, doi:10.1029/2008GB003316.

Frölicher, T. L., and F. Joos (2010), Reversible and irreversible impacts of greenhouse gas emissions in multi-century projections with the NCAR global coupled carbon cycle-climate model. *Clim. Dynam.*, *35*, 1439–1459, doi:10.1007/s00382-009-0727-0.

Frölicher, T. L., F. Joos, and C. C. Raible (2011), Sensitivity of atmospheric $CO_2$ and climate to explosive volcanic eruptions. *Biogeosci.*, *8*, 2317–2339, doi:10.5194/bgd-8-2957-2011.

Fung, I. Y., S. C. Doney, K. Lindsay, and J. John (2005), Evolution of carbon sinks in a changing climate. *Proc. Natl. Acad. Sci. USA*, *102* (32), 11201–11206, doi:10.1073/pnas.0504949102.

Gerlach, T. (2011), Volcanic versus anthropogenic carbon dioxide. *EOS Trans. AGU.*, *92*(24), 201, doi:10.1029/2011EO240001.

Gloor, M., J. L. Sarmiento, and N. Gruber (2010), What can be learned about carbon cycle climate feedbacks from the $CO_2$ airborne fraction? *Atmos. Chem. Phys.*, *10*, 7739–7751, doi:10.5194/acpd-10-9045-2010.

Gu, L., D. D. Baldocchi, S. C. Wofsy, J. W. Munger, J. J. Michalsky, S. P. Urbanskui, and T. A. Boden (2003), Response of a deciduous forest to the Mount Pinatubo eruption: Enhanced photosynthesis. *Science*, *299*, 2035–2038, doi:10.1126/science.1078366.

Houghton, R. A. (2003), Revised estimates of the annual net flux of carbon to the atmosphere from changes in land use and land management 1850-2000. *Tellus*, *55B*, 351–378, doi:10.1034/j.1600-0889.2003.01450.x.

Houghton, R. A. (2010), How well do we know the flux of CO2 from land-use change? *Tellus*, *62B*, 337–351, doi:10.1111/j.1600-0889.2010.00473.x.

Jones, C. D., and P. M. Cox (2001), Modelling the volcanic signal in the atmospheric $CO_2$ record. *Global Biogeochem. Cycles*, *15*, 453–465, doi:10.1029/2000GB001281.

Keeling, C. D., S. C. Piper, R. B. Bacastow, M. Wahlen, T. P. Whorf, M. Heimann, and H. A. Mijer (2001), Exchanges of atmospheric $CO_2$ and $^{13}CO_2$ with the terrestrial biosphere and ocean from 1978 to 2000. Global Aspects, SIO Reference Series, No. 01-06, Scripps Institution of Oceanography, San Diego, 88p.

Knorr, W. (2009), Is the airborne fraction of anthropogenic carbon dioxide increasing? *Geophys. Res. Lett.*, *36*, L21710, doi:10.1029/2009GL040613.

Le Quéré, C. et al. (2009), Trend in the sources and sinks of carbon dioxide. *Nat. Geosci.*, *2*, 831–836, doi:10.1038/ngeo689.

Meehl, G. A. et al. (2007), Global climate projections. In IPCC Climate Change 2007: The Physical Science Basis. Contribution of Working Group I to the Fourth Assessment Report of the Intergovernmental Panel on Climate Change, edited by S. Solomon, pp. 747–845, Cambridge Univ. Press Cambridge, United Kingdom and New York, NY, USA.

Mercado, L., N. Bellouin, S. Sitch, O. Boucher, C. Huntingford, M. Wild, and P. M. Cox (2009), Impact of changes in diffuse radiation on the global land carbon sink. *Science*, *458*, 1014–101, doi:10.1038/nature07949.

Pan Y. et al. (2011), A large and persistent carbon sink in the world's forests. *Science*, *333*, 988–993, doi:10.1126/science.1201609.

Rafelski, L. E., S. C. Piper, and R. F. Keeling (2009), Climate effects on atmospheric carbon dioxide over the last century. *Tellus B*, *61*(5), 718–731, doi:10.1111/j.1600-0889.2009.00439.x.

Raupach, M. R., J. G. Canadell, and C. Le Quéré (2008), Anthropogenic and biophysical contributions to increasing atmospheric $CO_2$ growth rate and airborne fraction. *Biogeosci.*, *5*, 1601–1613, doi:10.5194/bgd-5-2867-2008.

Robock, A. (2000), Volcanic eruptions and climate. *Rev. Geophys.*, *38*, 191–219, doi:10.1029/1998RG000054.

Rödenbeck, C., S. Houweling, M. Gloor, and M. Heimann (2003), $CO_2$ flux history 1982–2001 inferred from atmospheric data using a global inversion of atmospheric transport. *Atmos. Chem. Phys.*, *3*, 1919–1964, doi:10.5194/acp-3-1919-2003.

Sarmiento, J. L., M. Gloor, N. Gruber, C. Beaulieu, A. R. Jacobson, S. E. Mikaloff Fletcher, S. Pacala, and K. Rodgers (2010), Trends and regional distributions of land and ocean carbon sinks. *Biogeosci.*, *7*, 2351–2367, doi:10.5194/bg-7-2351-2010.

Schneider, B., L. Bopp, M. Gehlen, J. Segschneider, T. L. Frölicher, P. Cadule, P. Friedlingstein, S. C. Doney, M. J. Behrenfeld, and F. Joos (2008), Climate-induced interannual variability of marine primary and export production in three global coupled climate carbon cycle models. *Biogeosci.*, *5*, 597–614, doi:10.5194/bg-5-597-2008.

Steinacher, M., et al. (2010), Projected 21st century decrease in marine productivity: A multi-model analysis. *Biogeosci.*, *7*, 979–1005, doi:10.5194/bgd-6-7933-2009.

Stocker, B. D., K. Strassmann, and F. Joos (2011), Sensitivity of Holocene atmospheric $CO_2$ and the modern carbon budget to early human land use: Analyses with a process-based model. *Biogeosci.*, *8*, 69–88, doi:10.5194/bgd-7-921-2010.

Strassmann, K. M., F. Joos, and G. Fischer (2008), Simulating effects of land use changes on carbon fluxes: past contributions to atmospheric $CO_2$ increases and future commitments due to losses of terrestrial sink capacity, *Tellus B*, *60*, 583–603, doi:10.1111/j.1600-0889.2008.00340.x.

Thompson, D. W. J., J. M. Wallace, P. D. Jones, and J. J. Kennedy (2009), Identifying signatures of natural climate variability in time series of global-mean surface temperature: Methodology and insights. *J. Climate 22*, 6120–6141, doi:10.1175/2009JCLI3089.1.

Trenberth, K. E. (1997), The definition of El Niño. *Bull. Am. Meteorol. Soc.*, *78*, 2771–2777.

Trumbore, S. (2000), Age of soil organic matter and soil respiration: Radiocarbon constraints on belowground C dynamics, *Ecol. Appl.*, *10*(2), 99–411, doi:10.2307/2641102.

Wolter, K., and M. S. Timlin (1993), Monitoring ENSO in COADS with a seasonally adjusted principal component index. Proc. of the 17th Climate Diagnostics Workshop, Norman, OK, NOAA/NMC/CAC, NSSL, Oklahoma Clim. Survey, CIMMS and the School of Meteor., Univ. of Oklahoma, 52–57.

Wolter, K., and M. S. Timlin (1998), Measuring the strength of ENSO events—How does 1997/98 rank? *Weather*, *53*, 315–324, doi:10.1002/j.1477-8696.1998.tb06408.x.